Magneto-structural correlations in some molecular complexes

IR, Raman, SERS and DFT study of amoxicillin

Amoxicillin belongs to a class of antibiotics called penicillin. Amoxicillin is a moderate-spectrum, bacteriolytic, β-lactam antibiotic used to treat bacterial infections caused by susceptible microorganisms. Amoxicillin is effective against many different bacteria including *H. influenzae, N. gonorrhoea, E. coli, Pneumococci, Streptococci,* and certain strains of *Staphylococci*. It is usually the drug of choice within the class because it is better absorbed, following oral administration, than other β-lactam antibiotics. It acts by inhibiting the synthesis of bacterial cell wall, which are necessary to protect bacteria from their environment.

Due to the bio-molecular relevancy of amoxicillin, several spectroscopic studies can be found in the literature. A physicochemical characterization of amoxicillin and its beta-cyclodextrin complexes is shown in a recent study [1], including FTIR and NMR spectroscopy. Other spectroscopic methods employed for amoxicillin molecular characterization include, fluorescence [2], Raman and SERS [3].

Analytical detection approaches include UV spectrophotometry for amoxicillin determination in urine [4], NIR absorption combined with chemometrics as a method for the nondestructive determination of compound amoxicillin powder drug [5], chemo-luminescence [6] for determination of the compounds in pharmaceutical formulations and spiked plasma samples, or LC-MS/MS determination of amoxicillin in human plasma [7].

In the present study IR and Raman spectra of amoxicillin were assigned based on DFT calculations based on the hybrid B3LYP exchange-correlation functional, coupled with the standard 6-31G(d) basis set. The adsorption geometry of the amoxicillin molecule on colloidal silver surface was deduced from the SERS selection rules and the analysis of the calculated molecular electrostatic potential (MEP).

Instrumentation

The FTIR spectrum of amoxicillin powder was recorded at room temperature on a conventional Equinox 55 (Bruker Optik GmbH, Ettlingen, Germany) FTIR spectrometer equipped with an DTGS detector and an ATR setup with ZnSe crystall.

The FT-Raman spectrum was recorded in a backscattering geometry with a Bruker FRA

106/S Raman accessory equipped with a nitrogen cooled Ge detector. The 1064 nm Nd:YAG laser was used as excitation source, and the laser power measured at the sample position was 300 mW. All spectra were recorded with a resolution of 4 cm^{-1} by co-adding 32 scans.

The SERS spectrum was recorded using a DeltaNu Advantage spectrometer (DeltaNu, Laramie, WY) equipped with a doubled frequency Nd:YAG laser emitting at 532 nm. The laser power was 40 mW and the spectral resolution 10 cm^{-1}.

Computational details

The molecular geometry optimization, molecular electrostatic potential (MEP) and vibrational spectra calculations were performed with the Gaussian 03W software package [12] by using density functional theory (DFT) methods with B3LYP hybrid exchange-correlation functional [13, 14] and the standard 6-31G(d) basis set. No symmetry restriction was applied during geometry optimization. The vibrational frequencies were computed at the optimized geometry to ensure that no imaginary frequencies were obtained confirming that it corresponds to a local minimum on the potential-energy surface.

The assignment of the experimental frequencies are based on the observed band frequencies and intensity pattern of the Raman spectra and confirmed by establishing a one to one correlation between the observed and theoretical calculated frequencies. The calculated Raman activities (S_i) were converted to relative Raman intensities (I_i) using the following relationship [8-10]:

$$I_i = \frac{f(v_0 - v_i)^4 S_i}{v_i \left[1 - \exp\left(-\frac{hcv_i}{kT} \right) \right]} \tag{1}$$

where v_0 is the exciting laser wavenumber, v_i is the wavenumber of the i-th vibrational mode, c is the speed of light, h and k are Planck's and Boltzmann's constants and T is the temperature.

For the plot of simulated Raman spectrum, pure Lorentzian band shapes were used with the full width at half height (FWHH) of 15 cm^{-1}. The last column in both Tables contains the motions that contribute the most to different normal modes according to B3LYP method coupled with the 6-31G(d) basis set. The computed wavenumbers have been scaled by 0.9614 as proposed by Scott and Radom [18]. To aid in mode assignment, we based on the direct comparison between the experimental and calculated spectra by considering both, the frequency

sequence and intensity pattern, and by comparisons with vibrational spectra of similar compounds [19-22].

Results and discussion

After geometry optimization, vibrational frequencies were calculated for amoxicillin; no imaginary frequencies were obtained for the optimized geometry given in Figure 1, and thus, it represents a true minimum on the potential energy surface.
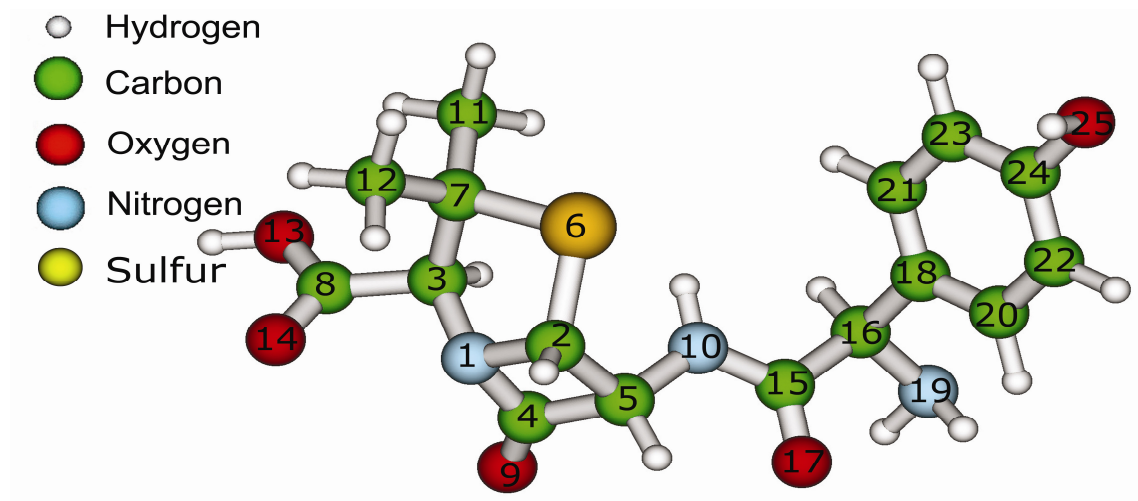

Figure 1. Optimized molecular structure and atom numbering scheme of amoxicillin.

Molecular electrostatic potential (MEP)

Molecular electrostatic potentials have been used for interpreting and predicting the reactive behavior of a wide variety of chemical systems in both electrophilic and nucleophilic reactions, the study of biological recognition processes and hydrogen bonding interactions [25, 26]. In this study, the amoxicillin atoms involved in the molecule adsorption to the silver surface are identified after analyzing the electrostatic potential map, as well. The MEP was calculated at the B3LYP/6-31G(d) optimized geometries, Figure 2 showing the calculated 3D electrostatic potential contour map of amoxicillin in atomic units, the electron density isosurface being 0.02 a.u..
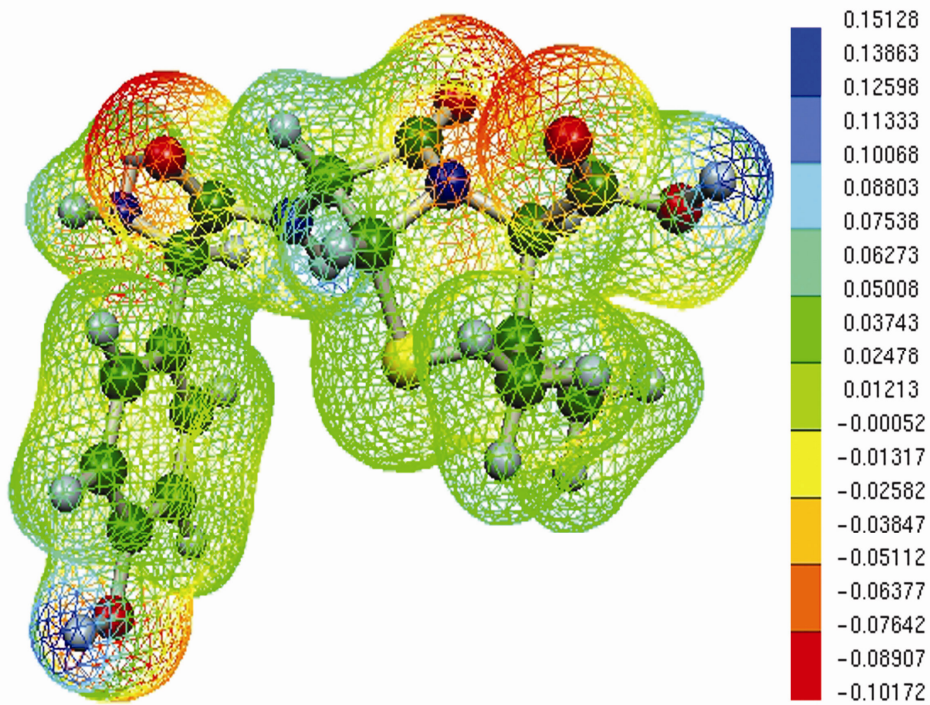
Figure 2. Calculated 3D molecular electrostatic potential contour map of amoxicillin, expressed in [au], as shown on the scale on the right side of the figure.

FTIR spectrum of amoxicillin

Fig.3 shows the experimental and calculated FTIR spectra of amoxicillin.

For amoxicillin, the C=O stretching vibrations show intense IR absorptions, due to the considerable change in the molecular dipole moment produced by this vibration mode. Thus, the 1773 and 1685 cm^{-1} bands, are due to the C8-O14 and C15-O17 stretching, as indicated by the theoretical DFT calculations. A detailed assignment of the experimental FTIR and calculated bands of amoxicillin is shown in Table 1.
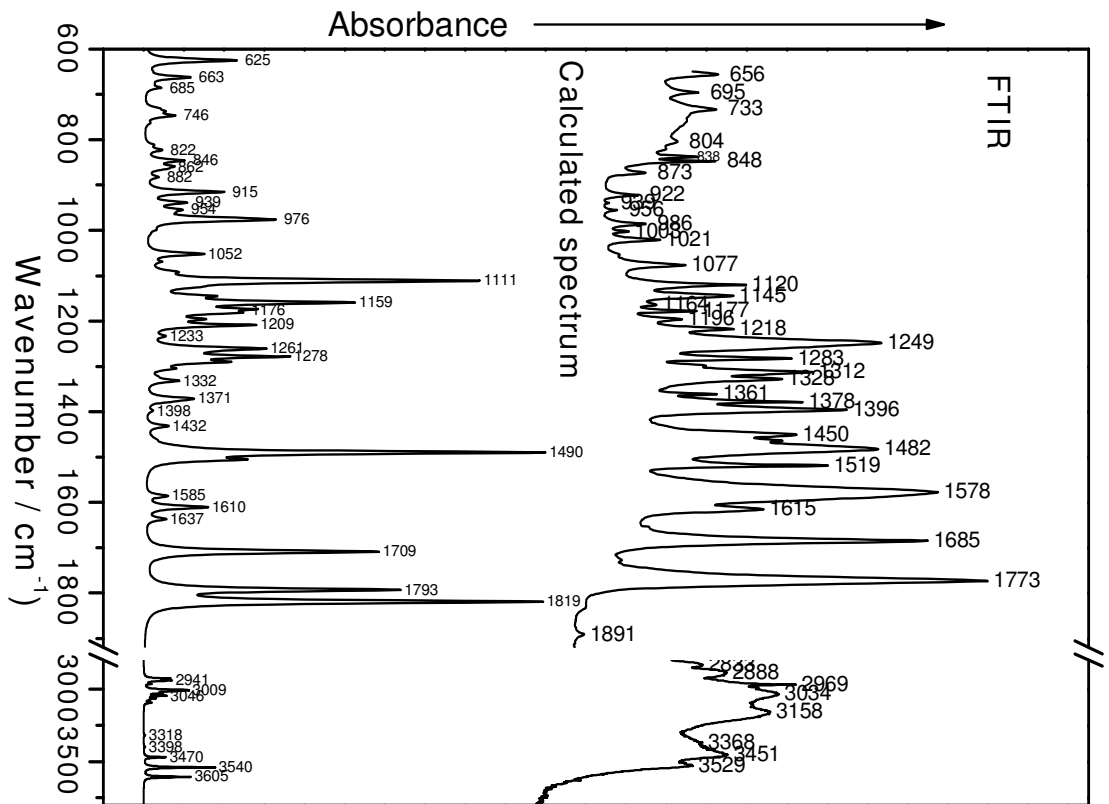
Figure 3. Experimental and calculated FTIR spectrum of amoxicillin.

Table 1. Experimental FTIR and theoretical calculated IR bands of amoxicillin, as well as their assignment.

Experimental wavenumbers (cm^{-1})	Calculated wavenumbers (cm^{-1})	Band assignment
FTIR/ATR	B3LYP	
3529	3540	ν(O13H)
3451	3470	ν(N10H)
3368	3398	ν_{as}(N19H$_2$)
3034	3046	ν_{as}(C21H,C23H)
2969	2963	ν(C3H)
1773	1793	ν(C8O14)+δ(O13H)
1685	1709	ν(C15O17)+δ(N10H)
1615	1610	ν(CC ring2)+δ(CH ring2)
1578	1585	ν(CC ring2)+δ(CH ring2)+δ(O25H)
1482	1490	ν(N10C15)+δ(N10H)+δ(C5H)
1450	1432	ν(CC ring2)+δ(CH ring2)+δ(O25H)+δ(C16H)
1396	1398	δ_s(CH$_3$)
1378	1371	δ(C3H)+δ(C8O$_2$H)+ν(C3C8)
1328	1332	ν(CC ring2)+δ(CH ring2)+δ(O25H)
1283	1278	ν(N1C3)+δ(N10H)+δ(N19H$_2$)+δ(CH)+δ(O13H)
1249	1233	δ(CH)
1218	1209	ν(C5C2,C5C4,C3N1)+δ(N10H)+δ(CH)
1177	1176	δ(N10H,N19H$_2$)+δ(CH)
1164	1159	δ(CH ring2)+δ(O25H)+δ(CH)+δ(N19H$_2$)
1120	1111	ν(O13C8)+δ(C8O14O13H)+δ(O13H)+δ(CH)
1021	1052	ν(CC,CN ring1)+ν(N1C4,C2N1)+δ(CH)+ δ(N19H$_2$)+δ(C12H$_3$)
986	976	δ(N19H$_2$)+op. bending CH ring2
956	954	δ(CH)+ν(C16NH$_2$)+δ(C15C16NH$_2$)
939	939	δ(C8C3HN1)+ν(C8C3H,C2C5)+δ(CH)+

		$\delta(O13H)+\delta(N19H_2)+\delta(C12H_3)$
922	915	$\nu(C15C16H,C2C5)+\delta(N19H_2)+\delta(C12H_3)$
873	862	ring2 breathing$+\delta(CH\ ring2)+\delta(CH)+\delta(N19H_2)$
848	846	op. bending CH ring2
834	822	op. bending CH ring2
733	746	$\delta(O13H)+\delta(C8O_2H)+\rho(CH_3)+\nu(C7C3)$
656	663	$\delta(O13H)$

ν- stretch, ν_s- symmetric stretch, ν_{as}- asymmetric stretch, δ- bending, ρ- rocking, γ-out-of-plane bending, def.-deformation, ip.-in plane, op.-out of plane, ring1: pyridine ring(N1-C2-S6-C7-C3); ring2: benzene ring(C18-C20-C21-C22-C23-C24)

As can be observed from Fig.3, other intense IR bands are those from 1482 cm^{-1}, assigned mainly to N10C15 stretching and N10H bending, and 1120 cm^{-1}, assigned mainly to O13C8 stretching and C8O14O13H bending vibration.

Raman and SERS spectra of amoxicillin

Figure 4 shows the FT-Raman, Raman DFT calculated and SERS spectra of amoxicillin.

A good correlation between the theoretically calculated and FT-Raman bands can be observed. A detailed assignment of the experimental FT-Raman and SERS as well as of the DFT calculated Raman bands of amoxicillin are shown in Table 2. The FT-Raman and SERS bands were visually correlated with the calculated spectrum, by taking into account, both, wavenumber value and relative intensity, and thus the assignment of the FT-Raman and SERS spectrum was performed.

Generally, the total symmetric vibration (breathing vibration) of aromatic rings shows high intensity Raman bands. In the FT-Raman spectrum of amoxicillin the total symmetric vibration of the benzene ring appears as a intense band at 852 cm^{-1}, in the calculated Raman spectrum being present at 862 cm^{-1}. Other intense FT-Raman bands in the amoxicillin spectrum are associated also with the benzene ring: 1618 cm^{-1}, due to ring C=C stretching, 1257 cm^{-1}, due to C-H bending and 1177 cm^{-1}, due to C-C stretching and C-H bending.
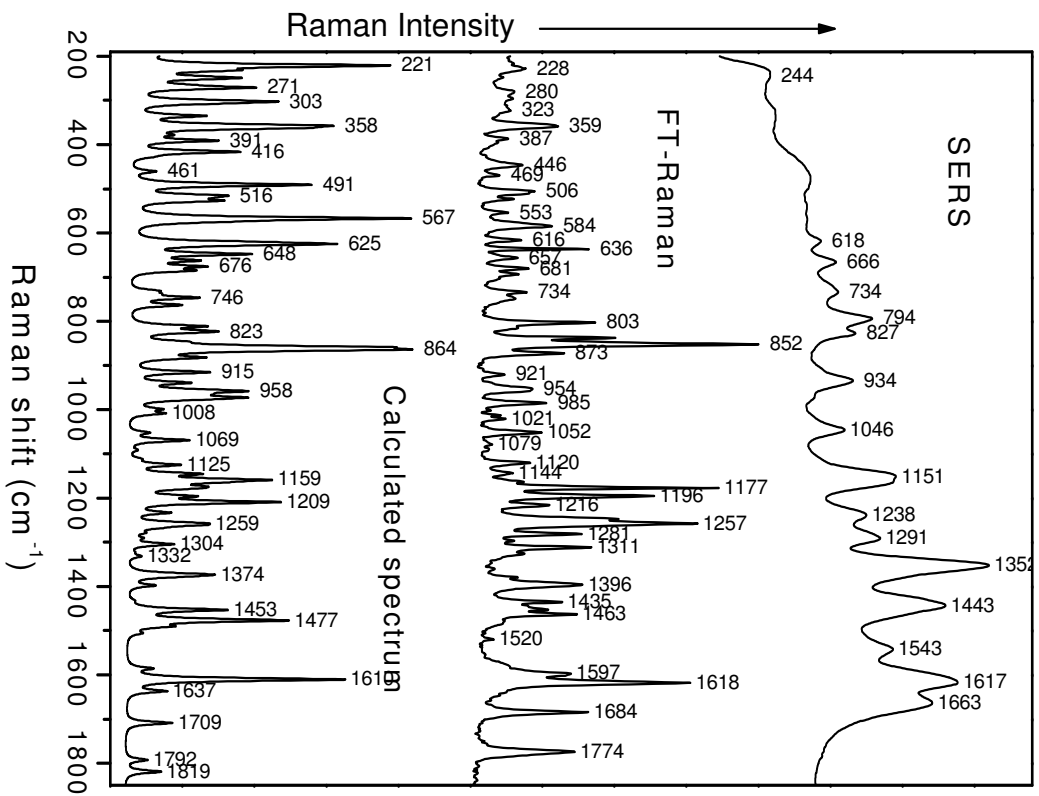
Figure 4. Experimental and simulated FT-Raman and SERS spectra of amoxicillin.

Table 2. FT-Raman, SERS, and theoretical calculated (B3LYP/6-31G(d)) bands of amoxicillin, as well as their assignment.

Experimental wavenumbers (cm⁻¹)		Calculated wavenumbers (cm⁻¹)	Band assignment
SERS	FT-Raman	B3LYP	
244	228	221	$\rho(NH_2)+\rho(CH_3)$
	280	271	$\rho(CNH_2)+$ op. ring2 deformation
	323	303	$\rho(CCH_3)+\delta(CCH_3)$
	359	358	$\rho(CCH_3)+\delta(CCH_3)$
	387	391	op. ring2, ring1 deformation+op. ring2, ring1 bending
	446	416	ip. ring1 deformation+$\delta(COH)$
	469	461	ip. ring1 deformation+$\delta(NH)+\delta(CCH_3)$
	506	491	op. ring2 bending+$\delta(NH)$
	553	516	op. ring2, ring1 deformation+op. ring2, ring1 bending
	584	567	$\delta(O13H)+\nu(C7S6)+\delta(C7CH_3)+\delta(CH_3)$
618	616	625	$\delta(O13H)+\delta(CH)+\delta(CH_3)$
666	636	648	ip. ring2 deformation+ring2 breathing
734	734	746	$\delta(O13H)+\delta(C8O_2H)+\rho(CH_3)+\nu(C7C3)$
794	803	811	ip. deformation
827	838	823	op. bending ring2+$\delta(CH$ ring2)
	852	864	ring2 breathing+$\delta(CH$ ring2)+$\delta(CH)+\delta(NH_2)$
934	921	915	$\rho(NH_2)+$ op. bending ring1+$\delta(CH)+\nu(C8C3)+\delta(OH)$
	954	958	$\rho(CH_3)+$op. bending CH ring2
	985	972	$\delta(CH)+\nu(C16NH_2)+\delta(C15C16NH_2)$
	1021	1008	$\rho(CH_3)$

1046	1052	1069	$\nu(C16NH_2)+\delta(NH_2)+\delta(CH)$
	1120	1125	$\delta(C12C7C11)+\rho(CH_3)$
1151	1177	1159	$\delta(CH)+\delta(OH)+\delta(CH\ ring2)+\nu(CC\ ring2)$
	1196	1209	$\delta(CH)+\delta(NH)+\nu(C5N10)$
1238	1257	1259	$\nu(C24OH)+\delta(CH\ ring2)$
			$\delta(CH)+\delta(NH)+\delta(CH\ ring2)+ip.\ ring2$
	1311	1304	deformation
1352	1396	1374	$\delta(CH)+\rho(NH_2)+\rho(NH_2CH)$
1443	1435	1453	$\delta_{as}(CH_3)$
	1463	1477	$\delta_{as}(CH_3)$
1617	1618	1610	$\nu(CC\ ring2)+\delta(CH\ ring2)$
1663	1684	1709	$\nu(C15O17)+\delta(C16H)+\delta(N10H)$
	1774	1792	$\nu(C8O14)+\delta(C3H)+\delta(O13H)$

ν- stretch, ν_s- symmetric stretch, ν_{as}- asymmetric stretch, δ- bending, ρ- rocking, γ-out-of-plane bending, def.-deformation, ip.-in plane, op.-out of plane, ring1: pyridine ring(N1-C2-S6-C7-C3); ring2: benzene ring(C18-C20-C21-C22-C23-C24)

Adsorption geometry of amoxicillin to the silver surface

According to the surface-selection rules [23, 24], the normal modes, with a change in polarizability component perpendicular to the surface are enhanced. Theoretically, the interaction of amoxicillin with the silver surface can be established through the, lone electron pairs of the O and N atoms, of the S atom, or through the π electrons of the rings.

The adsorption of amoxicillin to the silver surface is deduced based on the molecular electrostatic potential map and several marker bands. As can be seen in Figure 4 the highest electron density is located on oxygen atoms, thus the molecule is supposed to adsorb through the oxygen atoms. Benzene ring (ring 2) marker bands were identified at 852, 1177 and 1257 cm^{-1}. These bands are less represented in the SERS spectrum, thus the benzene ring does not lie in the near vicinity of the silver surface. Intense bands in the SERS spectra are observed at 1352 and 1443 cm^{-1} due to C-H bending and also at 1663 due to C=O stretching.

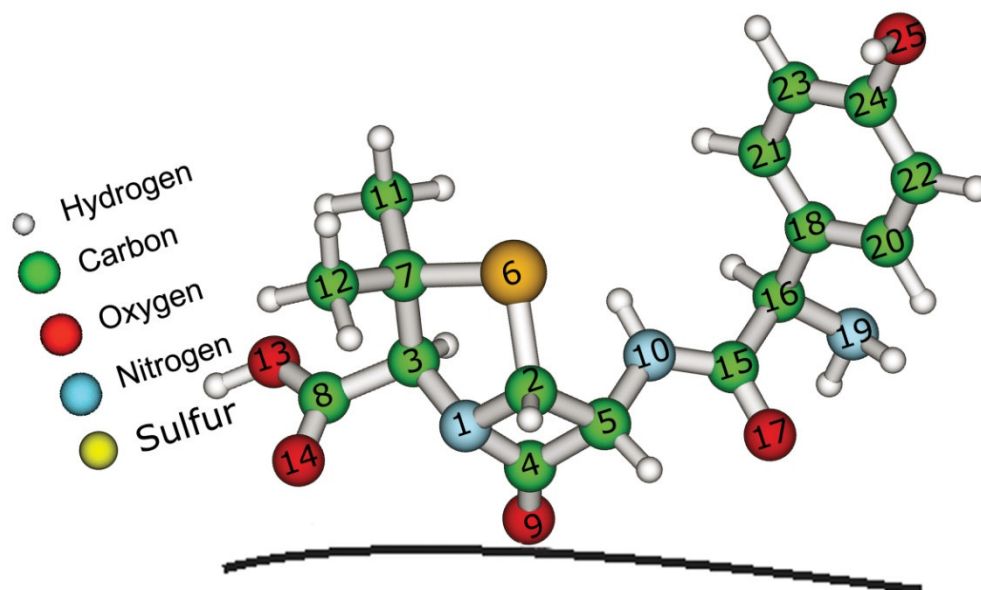Thus, the adsorption of the molecule was deduced as presented in Figure 5.

Figure 5. Schematically view of amoxicillin adsorption to the silver surface.

Conclusions

DFT calculations were employed for the geometry optimization, MEP and vibrational frequencies calculations of amoxicillin. The assignment of the FT-Raman and FTIR vibrational wavenumbers of amoxicillin was accomplished based on theoretical DFT calculations.

The adsorption geometry to the silver surface of amoxicillin was deduced from the SERS selection rules, several marker bands and the electrostatic potential map analysis.

References

[1]. A. Bebu, L. Szabó, N. Leopold, <u>C. Berindean</u>, L. David, Journal of Molecular Structure 993, 52, 2011

[2] Calborean, A., D. Maniu, V. Chis, T. Iliescu and V. K. Rastogi (2007), *Journal of Optoelectronics and Advanced Materials 9* (2007) *680-685*

[3] Elwalily, A. M., M. A. H. Elsayed, M. A. Korany and S. M. Galal, *Journal of Clinical Pharmacy and Therapeutics 17:(2), (1992) 101-105.*

[4] Qu, N., M. C. Zhu, H. Mi, Y. Dou and Y. L. Ren, *Spectrochimica Acta Part a-Molecular and Biomolecular Spectroscopy 70:(5), (2008) 1146-1151*

[5] Hasanpour, F., A. A. Ensafi and T. Khayamian , *Analytica Chimica Acta 670:(1-2) (2010) 44-50*

[6] Wen, A. D., T. J. Hang, S. N. Chen, Z. R. Wang, L. K. Ding, Y. Tian, M. Zhang and X. X. Xu, *Journal of Pharmaceutical and Biomedical Analysis 48:(3), (2008) 829-834*

[7] A. Pîrnău, V. Chiş¸ O. Oniga, N. Leopold, L. Szabo, M. Baias, O. Cozar, Vib. Spectrosc., 48 (2008) 289–296

[8] L.M. Gasheva, G. Kalinkova, E. Minkov and V. Krestev, Journal of Molecular Structure, Volume 115, March 1984

[9] Catherine Bisson-Boutelliez, Stephane Fontanay, Chantal Finance and Francine Kedzierewicz, AAPS PharmSciTech ,11 (2001) 574-81.

[10] N. Leopold, B. Lendl, J. Phys. Chem. B 107 (2003) 5723.

[11] Gaussian 03, Revision E.01, M. J. Frisch, G. W. Trucks, H. B. Schlegel, G. E. Scuseria, M. A. Robb, J. R. Cheeseman, J. A. Montgomery, Jr., T. Vreven, K. N. Kudin, J. C. Burant, J. M. Millam, S. S. Iyengar, J. Tomasi, V. Barone, B. Mennucci, M. Cossi, G. Scalmani, N. Rega, G. A. Petersson, H. Nakatsuji, M. Hada, M. Ehara, K. Toyota, R. Fukuda, J. Hasegawa, M. Ishida, T. Nakajima, Y. Honda, O. Kitao, H. Nakai, M. Klene, X. Li, J. E. Knox, H. P. Hratchian, J. B. Cross, V. Bakken, C. Adamo, J. Jaramillo, R. Gomperts, R. E. Stratmann, O. Yazyev, A. J. Austin, R. Cammi, C. Pomelli, J. W. Ochterski, P. Y. Ayala, K. Morokuma, G. A. Voth, P. Salvador, J. J. Dannenberg, V. G. Zakrzewski, S. Dapprich, A. D. Daniels, M. C. Strain, O. Farkas, D. K. Malick, A. D. Rabuck, K. Raghavachari, J. B. Foresman, J. V. Ortiz, Q. Cui, A. G. Baboul, S. Clifford, J. Cioslowski, B. B. Stefanov, G. Liu, A. Liashenko, P. Piskorz, I. Komaromi, R. L. Martin, D. J. Fox, T. Keith, M. A. Al-Laham, C. Y. Peng, A. Nanayakkara, M. Challacombe, P. M. W. Gill, B. Johnson, W. Chen, M. W. Wong, C. Gonzalez, and J. A. Pople,

Gaussian, Inc., Wallingford CT, 2004.

[13] P. Jankovics, T. Németh, J. Németh-Palotás, H. Koszegi-Szalai, Chromatographia, 68 (2008) S43.

[14] J.N. Latosińska, M. Latosińska, J. Kasprzak, Phys. Lett., 462 (2008) 295.

[15] R.G. Parr, W. Yang, Density-Functional Theory of Atoms and Molecules, Oxford University Press, New York, 1989

[16] K. Chruszcz, M. Baranska, K. Lewinski, L. M. Proniewicz, Vib. Spectroscop., 32 (2003) 199

[17] N. S. Goncalves, R. Cristiano, M. G. Piyyolatti, F. da Silva Miranda, J. Mol. Struct., 733 (2005) 53

[18] N. Sundaraganesan, S. Ayyappan, H. Umamaheswari, B. Dominic Joshua, Spectrochim. Acta A, 66 (2007) 17

[19] V. Chiş, A. Pîrnău, T. Jurcă, M. Vasilescu, S. Simon, O. Cozar, L. David, Chem. Phys., 36 (2005) 153

[20] L. Szabo, V. Chiş, A. Pirnău, N. Leopold, O. Cozar, Sz. Orosz, Vib. Spectrosc., 48, (2008) 297.

[21] H. Krawczyk, A. Pietras, A. Kraska, Spectrochim. Acta A, 66 (2007) 9.

[22] V. Chiş, A. Pîrnău, M. Vasilescu, R. A. Varga, O. Oniga, J. Mol. Struct. (Theochem) 831 (2008) 63.

[23] J.A. Creighton, Surf. Sci. 124 (1983) 209.

[24] M. Moskovits, J.S. Suh, J. Phys. Chem. 88 (1984) 5526.

[25] P. Politzer, J. S. Murray, in: Theoretical Biochemistry and Molecular Biophysics: A Comprehensive Survey, Vol. 2, Protein. D. L. Beveridge and R. Lavery, Eds., Adenine Press, Schenectady, NY, 1991, Chap. 13. Electrostatic Potential Analysis of Dibenzo–p–dioxins and Structurally Similar Systems in Relation to Their Biological Activities.

[26] P. Politzer, J. Murray, Theor. Chem. Acc, 108 (2002)

Synthesis and spectroscopic characterization of the novel heteropolyoxotungstates based on α-B-[BiIIIW9O33]9- units

Polyoxometalates (POMs) are a unique class of molecular metal-oxygen clusters. They consist of a polyhedral cage structure or framework bearing a negative charge and centrally located heteroatom(s) surrounded by the cage framework.

Trivacant Keggin fragments of $[\alpha\text{-B-X}^{III}W_9O_{33}]^{9-}$ (X-As, Sb, Bi) type are suitable building blocks for synthesis of large polyoxotungstates.

The species consist of two, three, four, six and twelve $[\alpha\text{-B-X}^{III}W_9O_{33}]^{9-}$ units which are linked by lanthanide cations in order to form new classes of material with a large anion cluster [1-5].

Transition metal substituted polyoxometalates have tracked attention because they can be rationally modified on the molecular level including size, shape, charge density, acidity, redox states, stability, solubility.

Polyoxometalates that are formed by self-assembly combine their nanoscopic size with the electronic, magnetic, or optical properties of the metal atoms, which should lead to interesting new materials. [6]

Two $K_{19}[Ce_3(H_2O)_8(BiW_9O_{33})_4WO_2(H_2O)]$ $2(Bi_4O_4)].48H_2O$ (**1**) and $K_{15}[Ce_2(H_2O)_2(BiW_9O_{33})$ $(W_5O_{18})_2].21H_2O$ (**2**) large cerium complexes were synthesized and characterized by chemical analysis along with FT-IR and UV-VIS spectroscopic methods.

Physical-chemical measurements

The carbon, nitrogen, hydrogen, sulphur and oxygen were analyzed on Vario El device.

Atomic absorption measurements for copper complexes were realized with an AAS-1 device at λ=320nm wavelength.

Infrared spectra were recorded on a Perkin-Elmer FT-IR 1730 Spectrophotometer over KBr solid samples in 4000- 400 cm-1 range.

Electronic absorption spectra were recorded in aqueous solution (10-5 M for ultraviolet and 10-3 for visible) using a Jasco V-530 spectrophotometer

Synthesis of the complexes

The reaction mechanism remains vague, even if worthy results were obtained regarding

complexes equilibrium which involves species formation even if a sort of semi-rational synthesis had been performed, starting from lacunary Keggin [XM11O39](12-n)-or [XM9O34](14-n)-.

Synthesis of trilacunary polyoxometalates used below as construction units of new complex polyoxometalates with metals from block f, respectively with some organostanic fragments had been performed using components, by acidulation utill pH 7-8, as shown in literature [7].

Synthesis of K19[(BiW9O33)4{WO2(H2O)]2; Ce3(H2O)8 (Bi4O4)]. 48H2O (1)

Na2WO4 (3.3 g, 10 mmol) was dissolved in 30 ml of H2O upon heating at 95 oC for 20 minutes. Then to the stirred solution was slowely added a solution of Bi(NO3)3· 5H2O (0.196 g, 0.405 mmol) in 1.54 ml of 6M HCl and the pH was adjusted to 7.5 by adding 2M KOH. The mixture was kept at 90 oC for an additional 20 minutes. Following filtration, was added Ce(NO3)3· 6H2O (0.469 g, 1 mmol) dissolved in 1,8 ml of 1M CH3COOH. Then was added a solution of 4g KCl in 15 mL water. A fine orange precipitate formed immediately, which was isolated by decantation and recrystallized from 5 ml of hot water. Orange needles formed after a few days. These crystals were stable in the mother liquor but slowely decayed in air.

Synthesis of K15[Ce2(H2O)2(BiW9O33)(W5O18)2]x21H2O (2)

Bi(NO3)3· 6H2O (0.43 g, 0.89 mmol) and Ce(NO3)3· 6H2O (0.67 g, 1.8 mmol) solids were dissolved in 4 mL aqueous 6M HCl with heating (solution 1). H2WO4 (4.2 g, 17 mmol) and KOH (2.5 g, 45 mmol) were were dissolved in hot water (60 mL at 80 oC) (solution 2). Solution 1 was added to solution 2 with stirring at room temperature. During the addition the pH was kept at ca. 7 by aqueous KOH, and finally adjusted to ca. 7.5. The resulting cloudy solution was filtered and the filtrate was cooled to 5 oC in a beaker. After two days wad obtained the pale orange microcrystals which was isolated by filtration and recrystallized from 20 ml of hot water.

Results and discussion

The elemental analysis results % found (calculated) for complex **1** are %K 5.38 (5.67), %Bi 12.42 (12.75), %W 53.52 (53.30), %Ce 3.02 (3.20), H2O 6.42 (6.59) and for complex **2** the results are %K 9.00 (9.63), %Bi 3.52 (3.43), %W 57.82 (57.38), %Ce 4.60 (4.43), H2O 6.61 (6.80).

The water amount was determined form the difference of initial and heated (at 120 0C, respectively calcination at 560 0C, for 30 minute) samples.

The elemental analysis and atomic absorption experimental results are in good agreement with the theoretical ones and with the proposed formulas.

FT-IR spectroscopy

Information about the metal ion coordination was obtained by comparing the IR frequencies of the ligands with those of the synthesized complexes (Figs. 1,2 and Table 1.).

In the spectrum of the cerium complex the band characteristic to sandwich type structures appear at 727 cm-1[8]. In the FT-IR spectra of the first complex (Fig. 1) can be observed the presence of valence bands characteristic for polyoxowolframate edifice, showing the stabilisation of the trilacunary polyoxoanion by cerium ions coordination [8].

In the FT-IR spectra of the second compound (Fig. 2) were also observed the valence bands characteristic for the polyoxowolframic edifice.

The band corresponding to antiphasic vibrations of terminal bonds W-Ot is expanded and shifted with 16 cm-1 towards higher frequencies suggesting a compressed bond [9,10].
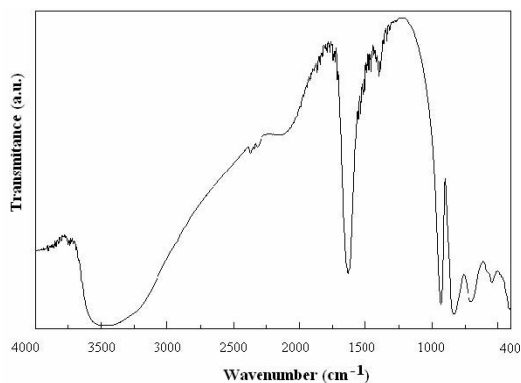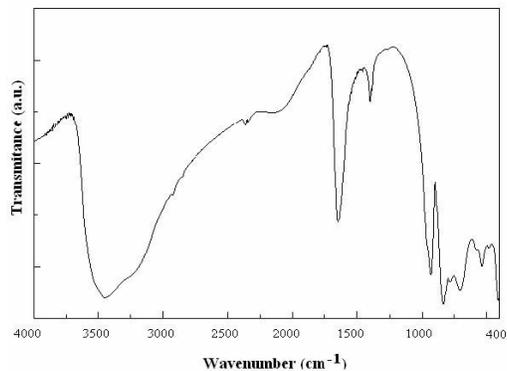

Fig.1. FT-IR spectrum of 1.

Fig. 2. FT-IR spectrum of 2.

Table 1. FT-IR data (cm^{-1}).

Vibration band	1	2
vasW=Ot	933 vs	934
vasW-Oe-W vasBi-Oi	871 sh, 831 vs	887 sh, 837 vs
vasW-Oe-W	796 sh, 700 vs	781 vs, 704 vs
δW-Oc,e-W	582 m, 544 m, 486 m	581 m, 538 m, 482 m

s-strong; m-medium; w-weak; b-broad;sh-shoulder

UV-VIS spectroscopy

In the visible domain, the electronic absorption spectra present absorption bands, characteristic for d→d or f→f transition. These bands are similar with those obtained in the poor crystalline field complexes [11].
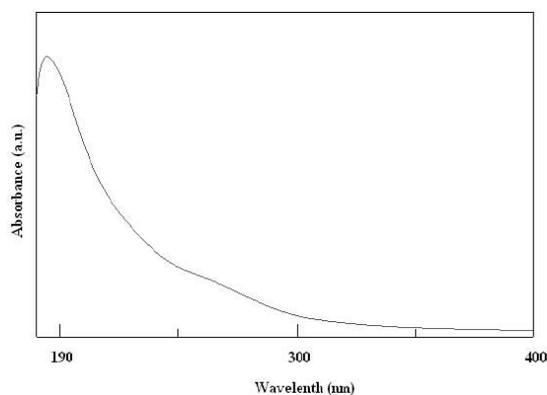
Fig. 3. UV electronic spectrum of K19[Ce3(H2O) 8(BiW9O33)4WO2(H2O)]2(Bi4O4)]48H2O.

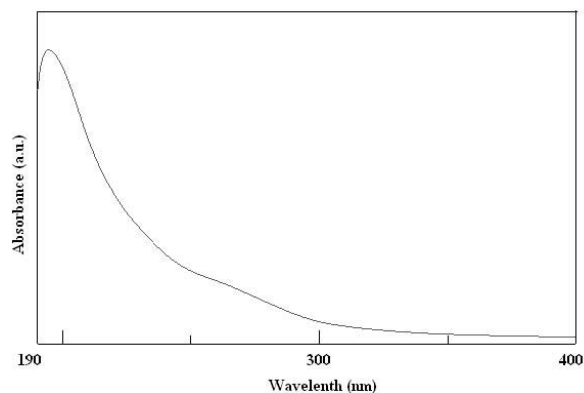*Fig. 4. UV electronic spectrum of K15[Ce2(H2O)2(BiW9O33)(W5O18)2].21H2O.*

In the ultraviolet spectra of the complexes were observed two types of bands: $\nu 1$ at ~195 nm attributed to the $p\pi(Ot) \rightarrow d\pi(W)$ charge transfer transition and $\nu 2$ at 244 nm, 289 nm (for complex **1**) and 249.5 nm and 299.5 nm (for complex **2**) which were assigned to the $p\pi(Oc,e) \rightarrow d\pi(W)$ charge transfer (Fig. 3).

A shoulder was observed in the visible spectra of both complexes at ~470 nm which was assigned to a metal-to-ligand charge transfer absorption [12,13].

Conclusions

Polyoxometalates are formed by policondensation of some oxoanionic species which contain metal transitional ions from V and VI groups (V(V), Nb(V),Ta(V), Mo(VI) and W(VI)).

Due to their definite stoichiometry, the present supported polyoxometalates can be converted to mixed metal oxide catalysts in a highly reproducible manner. Therefore, the polyoxometalates can also be used as a precursor for mixed metal oxide catalysts such as so- called Mitsubishi-type catalysts which are particularly useful for the oxidation of hydrocarbons such as propane .

Experimental data shown that in this sort of synthesis tree parameters are of extremely importance: concentration, pH and temperature.

The analytical and spectroscopic results were consistent with the proposed anion structures.

The obtained compounds are composed by cerium (III) cations, α-B-[BiW9O33]9- Keggin lacunary units and [W5O18]6- or Bi4O4 cluster. Every Ce (III) ion achieves a distorted square-antiprismatic eight-fold coordination by the oxygen atoms.
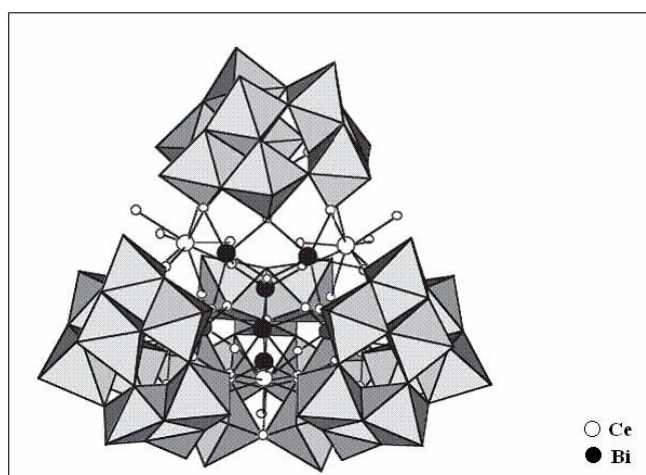

Fig. 5. Polyhedral representation of K19[(BiW9O33)4{WO2(H2O)]2Ce3(H2O)8(Bi4O4)].48H2O .

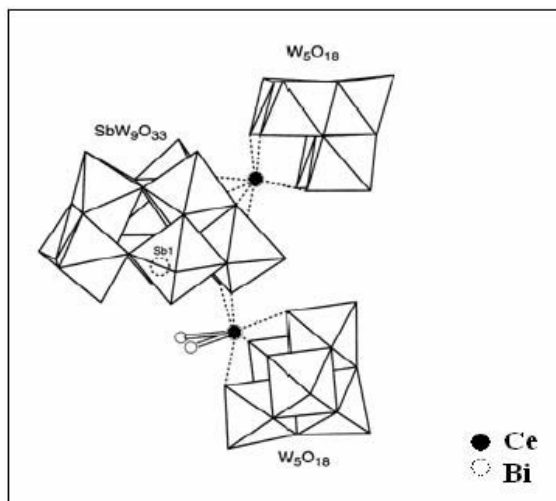*Fig.6. Polyhedral representation of K15[Ce2(H2O)2 (BiW9O33) (W5O18)2].21H2O complex.*

References

[1] D. Rusu, D. Mare, <u>C. Berindean</u>, A. Ungurean, O. Baban, L. David, Studia UBB Physica, Vol. 57 (LVII), 287-92, 2012.

 [2] Y. Jeannin, J. Cluster. Sci. **3**, 55 (1992).

[3] A. Muller, F. Peters, M. T. Pope, D. Gatteschi, Chem. Rev. **98**, 239 (1998).

[4] K. Kim, M. T. Pope, J. Chem. Soc. Dalton Trans. 986, 2001.

[5] G. Xue, J. Vaissermann, P. Gouzerh, J. Cluster Sci. **13**(3), 405 (2002).

[6] H. Naruke, T. Yamase, Bull. Soc. Jpn. **74**, 1289 (2001).

[7] H. Naruke, T. Yamase, Bull. Soc. Jpn. **75**, 1275 (2002).

 [8] G. Xue, J. Vaissermann, P. Gouzerh, J. Cluster Sci. **13**(3), 405 (2002).

[9] G. Socrates, Infrared and Raman Characteristic, Group Frequencies: Tables and Charts, third edition, Wiley, Chichester, 2001.

[10] H. Naruke, T. Yamase, Bull. Soc. Jpn. **74**, 1289 (2001).

[11] A. Marcu, A. Stanila, D. Rusu, M. Rusu, O.Cozar, L. David, J. Optoelectron. Adv. Mater. **9**(3), 741(2007).

[12] H. Naruke, T. Yamase, Bull. Soc. Jpn. **75**, 1275 (2002).

[13] M.S. Masond, O. H. Abd El-Hamid, Transition Metal Chemistry **14**, 233 (1989).

[14] A. R. Tomsa, L. Muresan, A. Koutsodimou, P. Falaras, M. Rusu, Polyhedron **22**, 2901 (2003).

[15] W. Hosny, Synth. React. Inorg. Met.-Org. Chem. **28**, 1029 (1998).

[16] M. Pope, A. Muller, Eds. Polyoxometalates. From Platonic Solids to Anti-Retroviral Activity, Kluwer Academic Publishers, Dordrecht, The Netherlands 1994.